June 2022

Numerical estimation of Pre-Swirl Stator efficiency

Andro BAKICA [a,1] and Nikola VLADIMIR [a]
[a] *Faculty of Mechanical Engineering and Naval Architecture, University of Zagreb, Croatia*

Abstract. This paper presents the investigation of a Pre-Swirl Stator (PSS) possible benefits on the ship powering system. Analysis of the PSS thrust augmentation is performed using the CFD simulations since the effects of turbulence and viscosity are important in the vicinity of the propeller. Direct propeller modelling is employed with the rotative region and propeller geometry present in the fluid domain. Two separate self-propulsion simulations are run, with and without the PSS, giving a clear correlation between the propulsive parameters and operability of the energy saving device. Results are also partially compared to the relevant experimental data. Hydrodynamic simulations are performed by means of open-source software OpenFOAM. The results show the PSS design to achieve a 4.7% decrease in the delivered power to the shaft which proves the design to be beneficial.

Keywords. Pre-Swirl Stator, CFD simulation, OpenFOAM, Self-propulsion

1. Introduction

Changing environmental regulations have enforced the need for a more energy efficient shipping industry with the expected incremental rise in the relevant measuring parameters. Previously, the IMO regulative referred only to the newly built vessels through the Energy Efficiency Design Index (EEDI), [1]. However, the latest regulations are expected to involve even the already built and sailing vessels through the defined Energy Efficiency Existing Ship Index (EEXI) [2] and this is creating a significantly more challenging task for the shipowners to satisfy in terms of limited improvements that can be done for an existing ship.

All this has prompted notable advances in the hydrodynamical improvements around the propeller through the so-called Energy Saving Devices (ESDs). The main purpose of the thrust augmented device is to reduce the delivered power to the propeller, but keeping the ship sailing at equal speed. This is enabled by exploiting the losses in the flow i.e. axial and rotational losses [3]. To reduce the axial losses, a duct type of ESD is frequently installed [4,5,6] by enabling the improved velocity distribution on the propeller inflow. Another relatively well-established ESD is the propeller boss cap fin which guarantees the reduction of the hub vortex and improves the fuel consumption in the range of 1-2% [7,8]. For the recovering of rotational losses, a Pre-Swirl Stator (PSS) can be fitted

[1]Corresponding Author: Andro Bakica, Faculty of Mechanical Engineering and Naval Architecture, University of Zagreb, Croatia; E-mail: andro.bakica@fsb.hr

[9,10]. The PSS creates a rotational velocity component opposite to the propeller rotation direction, thus increasing the load on the blades and reducing the amount of the rotational kinetic energy in the propeller slipstream. Furcas and Gaggero [11] developed a design procedure for the PSS using the genetic algorithm. For the optimal design the savings in the CFD numerical simulation showed even up to 8% in delivered power.

The current study features a PSS design on-board a very large crude oil carrier. The PSS is simulated in the CFD fluid solver for the cases with and without the ESD. In this manner, the possible savings can be easily deduced from the results. The resistance results are compared to the experimental data for various Froude numbers after which the full-scale mesh is prepared including the propeller. Propeller rotation is adjusted to match the ship resistance by using the dedicated rotation controller inside the simulation due to the non-linear interaction of propeller and the ship resistance.

The paper is divided into five sections as follows: second section explains the theoretical model behind the fluid simulations, third section describes the numerical model employed for the analysis, fourth section presents the results from the simulations and the fifth section outlines the study findings.

2. Mathematical model

Mathematical model is based on the Finite Volume (FV) discretisation in the arbitrary polyhedral framework of OpenFOAM [12]. Simulations are performed in the open-source version `foam-extend` where the in-house NavalHydro Pack [13,14] is employed. Special treatment of the free-surface is modelled with the Ghost Fluid Method (GFM) which ensures a sharp interface resolution. Fluid is assumed incompressible with the continuity equation as follows:

$$\nabla \bullet \mathbf{u} = 0, \tag{1}$$

where $\mathbf{u}$ is the fluid velocity. Furthermore, the momentum equation is written as:

$$\frac{\partial \mathbf{u}}{\partial t} + \nabla \bullet (\mathbf{u}(\mathbf{u})) - \nabla \bullet (\nu \nabla \mathbf{u}) = -\frac{1}{\rho} \nabla p_d + \nabla \bullet \mathbf{R}. \tag{2}$$

where $\rho(\mathbf{x})$ is the density of water or air, p_d is the dynamic pressure, ν is the kinematic viscosity and $\mathbf{R}$ is the Reynolds stress tensor. Two-phase flow and the definition of the free-surface locations is modelled using the Level Set (LS) formulation i.e. the signed distance from the interface between the two fluids:

$$\phi(\psi) = \tanh(\frac{\psi}{\varepsilon\sqrt{2}}), \tag{3}$$

where ψ is the signed distance field and ε is the smearing parameter set according to the mesh cell size near the free-surface. Coupling between the two equations is performed by a combination of a SIMPLE (outer corrector) loop inside a PISO loop (inner corrector) meaning that the pressure is corrected several times per each velocity correction [15].

Table 1. *KVLCC2 ship particulars.*

Hull parameters		
Length overall	L_{OA} [m]	325.5
Length between perpendiculars	L_{PP} [m]	320.0
Breadth	B [m]	58.0
Depth	H [m]	30.0
Design draught	T_d [m]	20.8
Ship speed	U [kn]	16.5

Propeller parameters		
Blade number		4
Diameter	D_P [m]	10.6
A_e/A_0		0.4288
Hub ratio		0.155

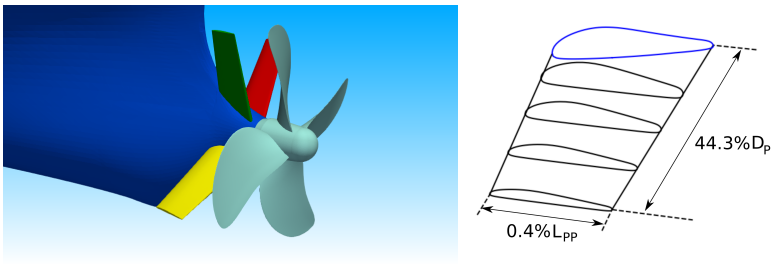

Figure 1. *Pre-Swirl Stator location on the ship (left) and geometry of particular fin (right).*

For the direct propeller simulation a rotative region is introduced inside the surrounding ship mesh with the General Grid Interface (GGI) [16]. This enables the interpolation of the flow variables at the merging interface between the two regions and does not require mesh size conformity, although similar sized cells are desirable for the interpolation procedure. Turbulence model used in this study is the $k-\omega$ SST due to its proven accuracy in adverse pressure gradient flows occurring at the ship wake [17]. For the waves diffracted from the ship hull, relaxation zones are introduced at the fluid domain boundaries to annul the possible reflection [18].

3. Numerical model

Ship geometry is a benchmark case KRISO Tanker KVLCC2 with particulars given in Table 1. PSS is fitted before the propeller plane as shown in Figure 1 with the geometry of a single fin also shown. Fluid domain for the hull is prepared in the following manner: $2 \cdot L_{PP}$ from inlet to ship, $2 \cdot L_{PP}$ from ship to to each of the side boundaries and $2.5 \cdot L_{PP}$ to the outlet boundary from the ship stern. In the vertical direction approximately 18 cells per expected wave height is made. Three different meshes are created: model scale mesh without the propeller and PSS, full-scale mesh with propeller and full-scale mesh with PSS and propeller. Model scale mesh is prepared with the symmetry plane and ensuring the y^+ value between 30 and 100. After verifying the results, full-scale mesh is created in a similar manner and scaled appropriately with the addition of the propeller region and PSS if necessary. However, for the full-scale mesh symmetry plane could not be employed due to inclusion of the propeller.

Surrounding mesh of the ship hull is shown in Figure 2 with the kelvin and free-surface refinement. Propeller and PSS region is shown in Figure 3 with the highlighted GGI region. Half-mesh domain for model-scale results consists of 3.0 M cells. Propeller

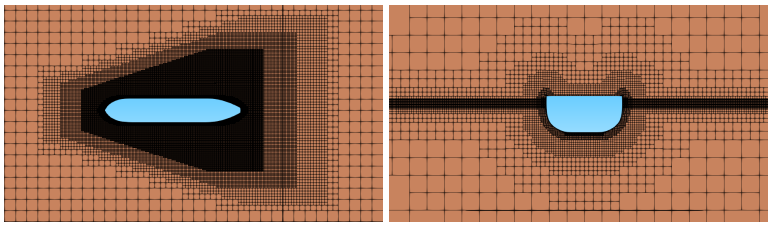

Figure 2. *Hull mesh.*

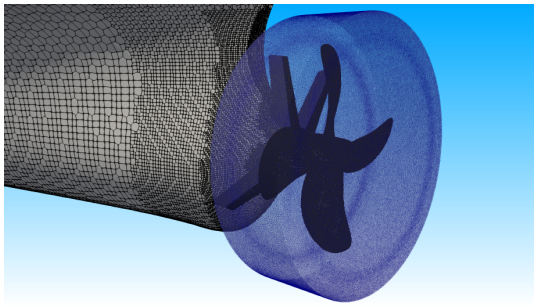

Figure 3. *Propeller mesh (GGI in blue).*

region is made using dedicated body-fitted mesh procedure to ensure a smooth surface on the blades and the propeller mesh counts 5.3 M cells. Lastly, the full-scale simulation with the propeller contains 11.3 M cells while the inclusion of the PSS accounts to roughly another 1.0 M cells.

Ship is allowed two degrees of freedom, pitch and heave. Floating body dynamic equation is solved as verified and validated in [19]. Propeller simulations are run first with the propeller being static, until all of the global variables (ship motion, drag force) and local (forces on PSS) converge. Then the propeller is turned on with the PI controller until balance of the thrust and ship resistance is accomplished. Same procedure is applied to the case with and without the PSS and the propeller parameters are then computed and compared. Second order accuracy schemes are set for spatial and time derivatives with limiters on velocity gradients for simulation stability. Time-step is adjusted to approximately 2° of propeller rotation depending on the converged propeller rotation.

4. Results and discussion

First set of results is presented for the model scale resistance comparison with the experiment. These results serve as a validation for an overall mesh geometry and numerical setup. Results are shown in Figure 4. The error for all Froude numbers is below 3%. Largest error is for the lowest Froude number while it slowly decreases as the velocity becomes higher. Wave field is shown in Figure 5 for the two Froude numbers. Design condition for the full-scale ship is equivalent to the Froude number of 0.151 where the error equals 0.71%. Overall, the results for the resistance have shown good agreement with the experiment at a wide range of ship speed conditions which justifies the numerical setup for further propeller simulations.

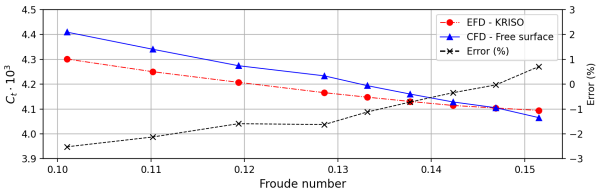

Figure 4. *Comparison of CFD and EFD results.*

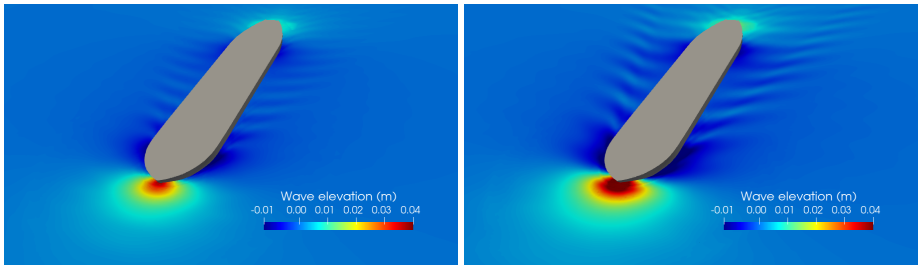

Figure 5. *Wave field for* $Fr = 0.119$ *(left) and* $Fr = 0.142$ *(right) in model scale.*

Following the model-scale results, simulations are run with and without the PSS, including the propeller in both cases. Convergence of the propeller rotation can be seen in Figure 6. Rotation rate for the case w/o and with PSS equals 70.14 and 67.92 rpm, respectively. However, this does not effectively mean that the design is valid since the delivered power has an utmost importance when assessing the ESD design. When comparing the $10 \cdot K_Q$ parameter for the case w/o and with PSS the values are 0.164 and 0.172, respectively. As expected from the PSS theoretical background, the counter rotational velocity component produced by the PSS creates a higher loading on the propeller blades increasing the torque. It is through this interaction of propeller rotation rate and the blade loads that the savings are accomplished. Consequently, the amount of rotational energy behind the propeller is lowered. For this particular PSS design, computed savings are equal to 4.7% in delivered power, 2258 kW and 2152 kW for cases w/o and with PSS, respectively. Pressure on the propeller blade is similar in both cases as shown in Figure 7, with the bottom blade root carrying higher loads at the leading edge. Suction side of the propeller tip is given in Figure 8 where in both cases there is a significant pressure drop showing possibility of propeller tip vortex cavitation. However, shape and size of the low pressure zone is similar in both cases.

The PSS forces are below 1% of the entire ship resistance when the propeller is operational. This is important to mention since the calm-water resistance of the PSS without the propeller is often commented in the literature. PSS and the propeller should be observed as a single system and when evaluating the drag of the PSS it should always be observed only when the propeller is operational since the flow field drastically changes. This can be clearly seen in Figure 9. Overall, the current results have shown the PSS design to be beneficial in terms of fuel consumption with the thrust gains overcoming the PSS additional drag and increase in the torque loading on the blades.

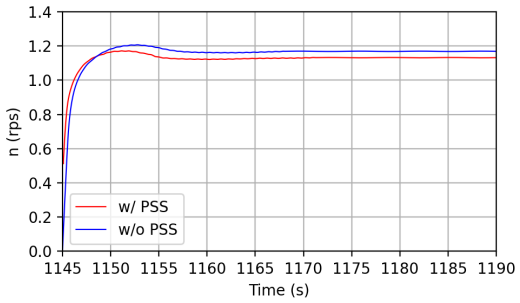

Figure 6. *Convergence of the propeller rotation rate.*

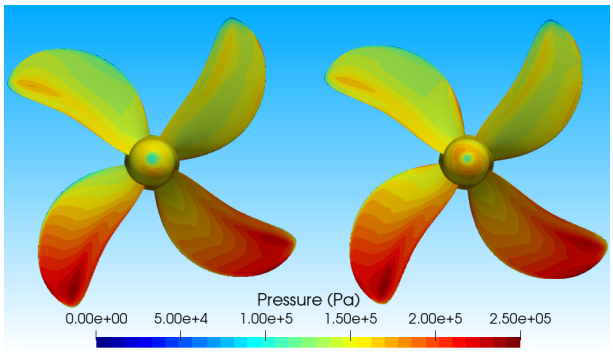

Figure 7. *Propeller surface pressure, left - without PSS, right - with PSS.*

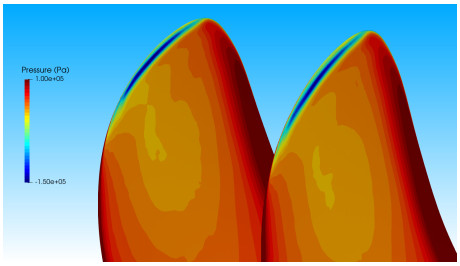

Figure 8. *Pressure drop at the propeller blade tip, left - without PSS, right - with PSS.*

5. Conclusion

This study presented the evaluation of the PSS design on a VLCC ship hull for $Fr = 0.151$. The numerical simulations are performed in the CFD including the fluid viscosity and turbulence while assuming incompressibility. Inside the fluid domain, two phase flow is modelled with the LS formulation and GFM to account for the sharp interface discontinuity numerical problems. Self-propulsion simulations are modelled with the direct propeller computation enabled through the rotative propeller GGI region. The flow quantities are interpolated at the interface which permits one part of the mesh to be movable with respect to the surrounding hull mesh.

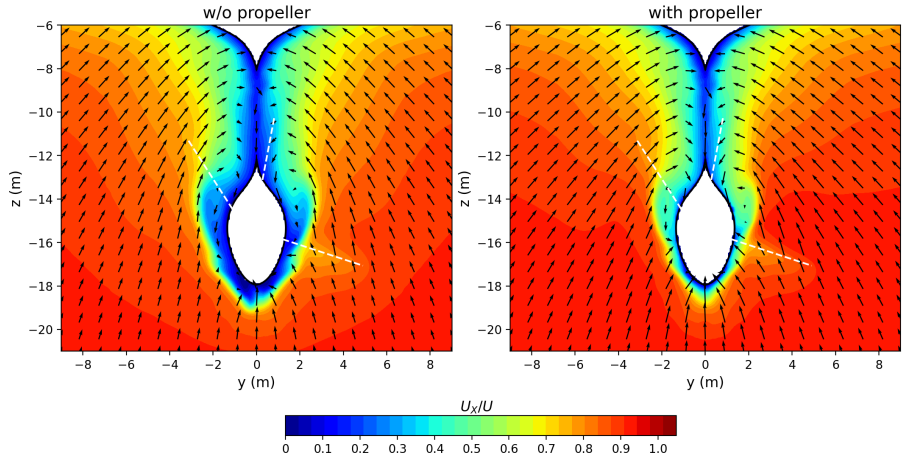

Figure 9. *Velocity contours with and without propeller between PSS and propeller plane.*

Two sets of simulations are prepared and solved for at model scale and full-scale. First, model scale results are compared to the experimental values for resistance in order to verify the computational model of this study. For a wide range of Froude numbers, the errors are below 3% with the design and subsequently studied condition with the PSS at $Fr = 0.151$ having an error of 0.71%. Given the sufficiently accurate results at model scale, the same mesh methodology is applied at full-scale with the inclusion of the propeller. Two simulations are prepared with and without the PSS before the propeller plane so that the efficiency of the thrust augmented device can be studied. Computations are run until the thrust and ship resistance force are in balance. From the results with and w/o PSS, the propeller torque is increased since the PSS creates a counter velocity component opposed to the propeller rotation. However, this enables the same ship speed for the lower rotation rate which altogether reduces the amount of delivered power to the shaft. In this case, the estimated savings are equal to 4.7% which shows the potential of the PSS device.

Following with the new IMO regulations for existing ships through EEXI, ESDs show a promising novelty for the improvement of the ship efficiency especially due to the ease of retrofitting on the existing ships.

Acknowledgement

This research was supported by the Croatian Science Foundation under the project Green Modular Passenger Vessel for Mediterranean (GRiMM), (Project No. UIP-2017-05-1253).

References

[1] IMO. Resolution MEPC.203(62) Inclusion of regulations on energy efficiency for ships in MARPOL Annex VI.; 2011.

[2] IMO. MEPC 67 Further shipping GHG emission reduction measures adopted in MARPOL Annex VI.; 2021.

[3] Sakamoto N, Kume K, Kawanami Y, Kamiirisa H, Mokuo K, Tamashima M. Evaluation of hydrodynamic performance of pre-swirl and post-swirl ESDs for merchant ships by numerical towing tank procedure. Ocean Engineering. 2019;178(February):104-33. Available from: https://doi.org/10.1016/j.oceaneng.2019.02.067.

[4] Gokce MK, Kinaci OK, Alkan AD. Self-propulsion estimations for a bulk carrier. Ships and Offshore Structures. 2019;14(7):656-63. Available from: https://doi.org/10.1080/17445302.2018.1544108.

[5] Zhao QX, Guo CY, Zhao DG. Study on self-propulsion experiment of ship model with energy-saving devices based on numerical simulation methods. Ships and Offshore Structures. 2015;10(6):669-77. Available from: http://dx.doi.org/10.1080/17445302.2014.945765.

[6] Bakica A, Vladimir N, Jasak H, Kim ES. Numerical simulations of hydrodynamic loads and structural responses of a Pre-Swirl Stator. International Journal of Naval Architecture and Ocean Engineering. 2021;13:804-16. Available from: https://doi.org/10.1016/j.ijnaoe.2021.09.002.

[7] Lim SS, Kim TW, Lee DM, Kang CG, Kim SY. Parametric study of propeller boss cap fins for container ships. International Journal of Naval Architecture and Ocean Engineering. 2014;6(2):187-205. Available from: http://dx.doi.org/10.2478/IJNAOE-2013-0172.

[8] Mizzi K, Demirel YK, Banks C, Turan O, Kaklis P, Atlar M. Design optimisation of Propeller Boss Cap Fins for enhanced propeller performance. Applied Ocean Research. 2017;62:210-22. Available from: http://dx.doi.org/10.1016/j.apor.2016.12.006.

[9] Kim JH, Choi JE, Choi BJ, Chung SH, Seo HW. Development of Energy-Saving devices for a full Slow-Speed ship through improving propulsion performance. International Journal of Naval Architecture and Ocean Engineering. 2015;7(2):390-8. Available from: http://dx.doi.org/10.1515/ijnaoe-2015-0027.

[10] Koushan K, Krasilnikov V, Nataletti M, Sileo L, Spence S. Experimental and numerical study of pre-swirl stators PSS. Journal of Marine Science and Engineering. 2020;8(1).

[11] Furcas F, Gaggero S. Pre-swirl stators design using a coupled BEM-RANSE approach. Ocean Engineering. 2021;222(January):108579. Available from: https://doi.org/10.1016/j.oceaneng.2021.108579.

[12] Jasak H, Weller HG. Application of the finite volume method and unstructured meshes to linear elasticity. Int J Numer Methods Eng. 2000;48:267-87.

[13] Vukčević V, Jasak H, Malenica S. Decomposition model for naval hydrodynamic applications, Part I: Computational method. Ocean Eng. 2016;121:37-46.

[14] Vukčević V, Jasak H, Malenica S. Decomposition model for naval hydrodynamic applications, Part II: Verification and validation. Ocean Eng. 2016;121:76-88.

[15] Jasak H, Uroić T. Practical Computational Fluid Dynamics with the Finite Volume Method. In: Modeling in Engineering Using Innovative Numerical Methods for Solids and Fluids. Springer; 2020. p. 103-61. Available from: http://link.springer.com/10.1007/978-3-030-37518-8.

[16] Beaudoin M, Jasak H. Development of a Generalized Grid Interface for Turbomachinery simulations with OpenFOAM. In: Open Source CFD International Conference; 2008. p. 1-11. Available from: papers3://publication/uuid/81CCD00D-DF48-4595-B591-C577955CEA06.

[17] Bakica A, Gatin I, Vukčević V, Jasak H, Vladimir N. Accurate assessment of ship-propulsion characteristics using CFD. Ocean Engineering. 2019;175:149-62.

[18] Jasak H, Vukčević V, Gatin I. Numerical Simulation of Wave Loads on Static Offshore Structures. In: CFD for Wind and Tidal Offshore Turbines. Springer Tracts in Mechanical Engineering; 2015. p. 95-105.

[19] Gatin I, Vukčević V, Jasak H, Rusche H. Enhanced coupling of solid body motion and fluid flow in finite volume framework. Ocean Engineering. 2017;143(December 2016):295-304.